Proceedings of the ASME 29th International Conference on Ocean, Offshore and Arctic Engineering
OMAE2010
June 6 - June 11, 2010, Shanghai, China

OMAE2010-20335

NUMERICAL INVESTIGATION OF SLOSHING IN A TANK, STATISTICAL DESCRIPTION OF EXPERIMENTS AND CFD CALCULATIONS

Bogdan Iwanowski*
FORCE Technology Norway AS
Claude Monets alle 5
1338 Sandvika
Norway
Email: boi@force.no

Marc Lefranc
FORCE Technology Norway AS
Email: mrl@force.no

Rik Wemmenhove
FORCE Technology Norway AS
Email: riw@force.no

ABSTRACT

Numerical study of liquid dynamics in an LNG tank is presented. The available data from large scale (1:10) sloshing experiments of 2D section of an LNG carrier reveal large scatter in recorded values of peak pressures. The experimental data is analysed from statistical point of view in order to obtain distributions of the pressure peaks. Then the entire experimental data record is reproduced numerically by CFD simulations and it is shown that pressure peaks obtained numerically display scatter of values as well. A statistical description of the numerically obtained record is provided and compared with description derived from the experimental data.

The applied CFD code ComFLOW solves Navier-Stokes equations and uses an improved Volume of Fluid (iVOF) method to track movement of fluid's free surface. Two different fluid models, single-phase (liquid+void) and two-phase (liquid+compressible gas) can be applied, the latter model being capable of simulating bubbles and gas entrapped in liquid. For low tank filling rate discussed in the paper (10%) the single-phase approach is sufficient. Comparison of statistical properties of experimental and numerical records is offered.

INTRODUCTION

Sloshing of liquids in cargo tanks of an LNG carrier oscillating in waves is a problem that must be addressed by marine engineers. The sloshing phenomenon is characterized by high pressure peaks due to fluid impact on the tank's walls or internal pipelines. The excessive load can lead to local structural damage of the tank's membrane, auxiliary internal installations and ultimately the tank's wall.

Various methods are in use for computational estimations of fluid pressures due to sloshing [1–6], and that list is by no means exhaustive. It can be also mentioned that during the 1^{st} ISOPE SDD Symposium [7] a number of interesting, currently state-of-art, approaches have been presented, including the approach employing the ComFLOW code used by authors.

The real sloshing loads occur in offshore situations and are of stochastic nature. It is therefore of interest whether some of statistical properties can be reproduced computationally. A statistical description of measured and computed sloshing pressures is presented in this paper. Long computational runs, matching the length of available experimental records, have been completed in order to gather the necessary information. The analysis leads to several observations which can be of value to researchers working with sloshing problems.

THE COMFLOW PROGRAM

The 3D Computational Fluid Dynamics solver ComFLOW has been developed by University of Groningen, The Netherlands. A local height function has been introduced as an improvement over the original VOF algorithm [8]. The code is being actively developed and has been thoroughly verified against

*Address all correspondence to this author.

experiments during Joint Industry Projects SAFE-FLOW and ComFLOW-2, [9].

The ComFLOW code has already been applied to the sloshing problem [4,5,10–12] and a comparison with the experimental results was presented.

MATHEMATICAL MODELS

The ComFLOW program can employ one of two basic physical models, either single-phase (liquid+void) or two-phase fluid flow (liquid+compressible gas). The latter model seems to be necessary for sloshing calculations with higher fluid filling rates. It is understood that "liquid" is an incompressible heavy fluid, such as water or liquefied natural gas (LNG). The compressible gas phase can be either air or an LNG vapour.

The mathematical models used in single-phase ComFLOW have been described elsewhere [13, 14] and only a brief description is provided below. Two-phase flow results are not presented in this paper, and therefore description of this model is omitted, but can be found in [3, 10].

Single-Phase Flow

Flow of an incompressible fluid, in an arbitrary three-dimensional domain can be found by solving continuity equation, Eqn. (1), together with Navier-Stokes equations describing conservation of momentum, Eqn. (2):

$$\nabla \cdot \mathbf{u} \;=\; 0 \qquad (1)$$

where $\mathbf{u} \;=\; (u,v,w)$ is fluid's velocity vector.

$$\frac{\partial \mathbf{u}}{\partial t} \;+\; \mathbf{u} \cdot \nabla \mathbf{u} \;=\; -\frac{1}{\rho} \nabla p \;+\; \frac{\mu}{\rho} \nabla \cdot \nabla \mathbf{u} \;+\; \mathbf{G} \qquad (2)$$

with p being fluid's pressure, ρ its constant density and μ its constant dynamic viscosity coefficient. Further, t is time and $\mathbf{G} = (G_x, G_y, G_z)$ is an external body force, for example gravity.

Second Order Upwind Differencing

The nonlinear convective terms in Navier-Stokes equations require special attention. The often used 1^{st} order upwind differencing scheme introduces a large amount of artificial dissipation. Therefore, the 2^{nd} order upwind differencing scheme (hereafter denoted as **B3**) has been implemented in ComFLOW in order to limit amount of numerical damping caused by the upwind differencing itself. Both 1^{st} and 2^{nd} order time integration schemes must satisfy the usual CFL-number and diffusive-number stability criteria.

The 2^{nd} order scheme gives less numerical damping, but also requires a change in time integration algorithm. Three time levels of variables and Adams-Bashforth time integration scheme are necessary to assure stability. It is also noted that calculations with the **B3** scheme call for much smaller computational time step and are typically 3-10 $\times$ slower than with the 1^{st} order scheme.

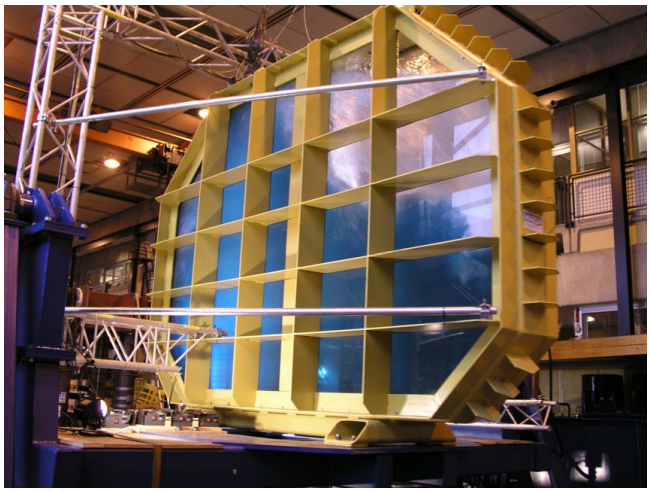

Figure 1. Experimental sloshing tank prepared by MARIN

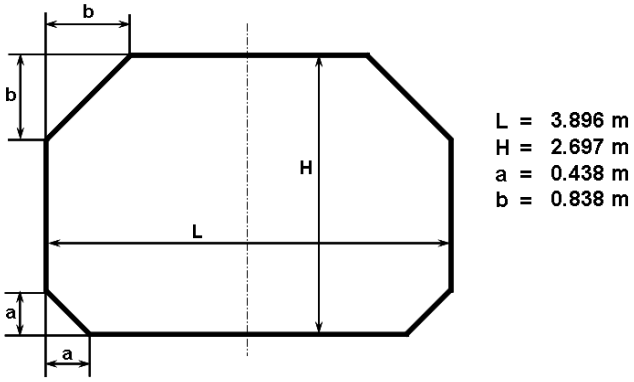

Figure 2. Experimental sloshing tank, main dimensions

THE SLOSHING EXPERIMENTS

Large scale (1:10) sloshing experiments were performed during the ComFLOW-2 JIP, with main objective of providing validation material for the ComFLOW code. The used prismatic tank, Fig. 1, was a 2D slice of a typical LNG carrier. Main dimensions of the experimental tank are shown in Fig. 2. More detailed description of the experiments can be found in [12, 15].

The experimental program included sway and roll motions of the tank (separate and combined), regular and irregular excitations, and several fill levels. The recorded time-value traces included data about the tank motion itself, water height at 12 fluid height probes and fluid pressure at 14 pressure sensors. The

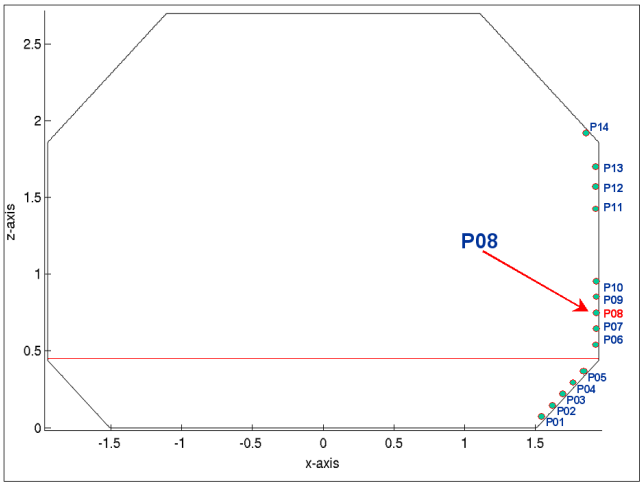

Figure 3. Locations of pressure sensors for 10% filling rate

local wave heights are not presented in this paper, but [4] can be consulted.

This paper discusses regular sway motions of the tank filled at 10%. Locations of the fluid pressure sensors for the 10% filling rate are shown in Fig. 3. Fluid pressures at **P08** location are analysed; for the considered fill rate, the sloshing pressures at this sensor location are of mostly dynamical kind.

Kinematics of the tank Motion

Motion of the tank itself, as modelled for numerical simulation of sloshing in ComFLOW, should be the same as recorded during the experiment. Time traces of tank's displacement are available from the experiments. However, description of moving coordinate system in ComFLOW requires time traces of tank's velocity and acceleration as well.

Although experimental time traces of the tank's displacement look quite regular, its velocity and acceleration, if derived by simple central finite differences, contain many peaks, [4]. Such numerically induced peaks can be removed by some kind of pre-processing, but it has been decided that the original (experimental) tank's displacement signal should not be touched (no filtering or smoothing techniques should be applied). A carefully designed procedure, the generalized finite differences, has been applied in order to derive the necessary kinematical variables, as described in [4, 11].

COMPUTATIONAL SETUP

The experimental tank, Fig. 1, was designed as a nearly two-dimensional container. Internal space between the transparent walls was 0.3 [m] only, roughly 10 $\times$ smaller than other tank's main dimensions. The concept was to validate sloshing capabilities of ComFLOW with less complex and considerably cheaper

Figure 4. Computational grid, 2D calculations

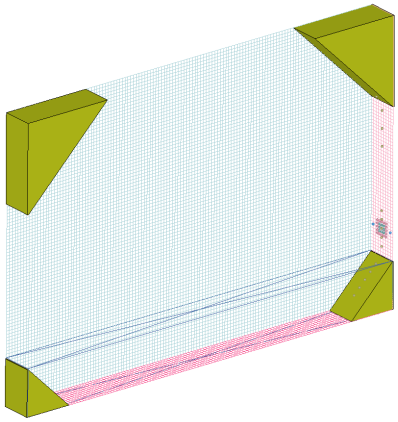

Figure 5. Computational grid, 3D calculations

(computationally) 2D flow cases. The ComFLOW grid for 2D computations is shown in Fig. 4 and locations of the pressure sensors are depicted as dots visible along the right-low chamfer and right vertical wall. The 2D geometry is an idealization of the experimental setup.

In order to verify the two-dimensionality assumption, the test has been also run in 3D mode. The applied computational grid is displayed in Fig. 5, and that geometry is an exact replica of the experimental tank. The computational pressure sensors have been placed at the centre-plane, as in the experiments. Additionally, a sub-panel of computational pressure sensors was placed in the neighbourhood of the **P08** point; this panel is barely legible in Fig. 5, but will be discussed later in this article.

Uniform computational grids have been used for both 2D and 3D calculations, $130 \times 1 \times 90$ and $130 \times 9 \times 90$ computational cells, respectively. The calculations with the single-phase fluid flow model (liquid only) and 2^{nd} order **B3** upwind differencing scheme were performed.

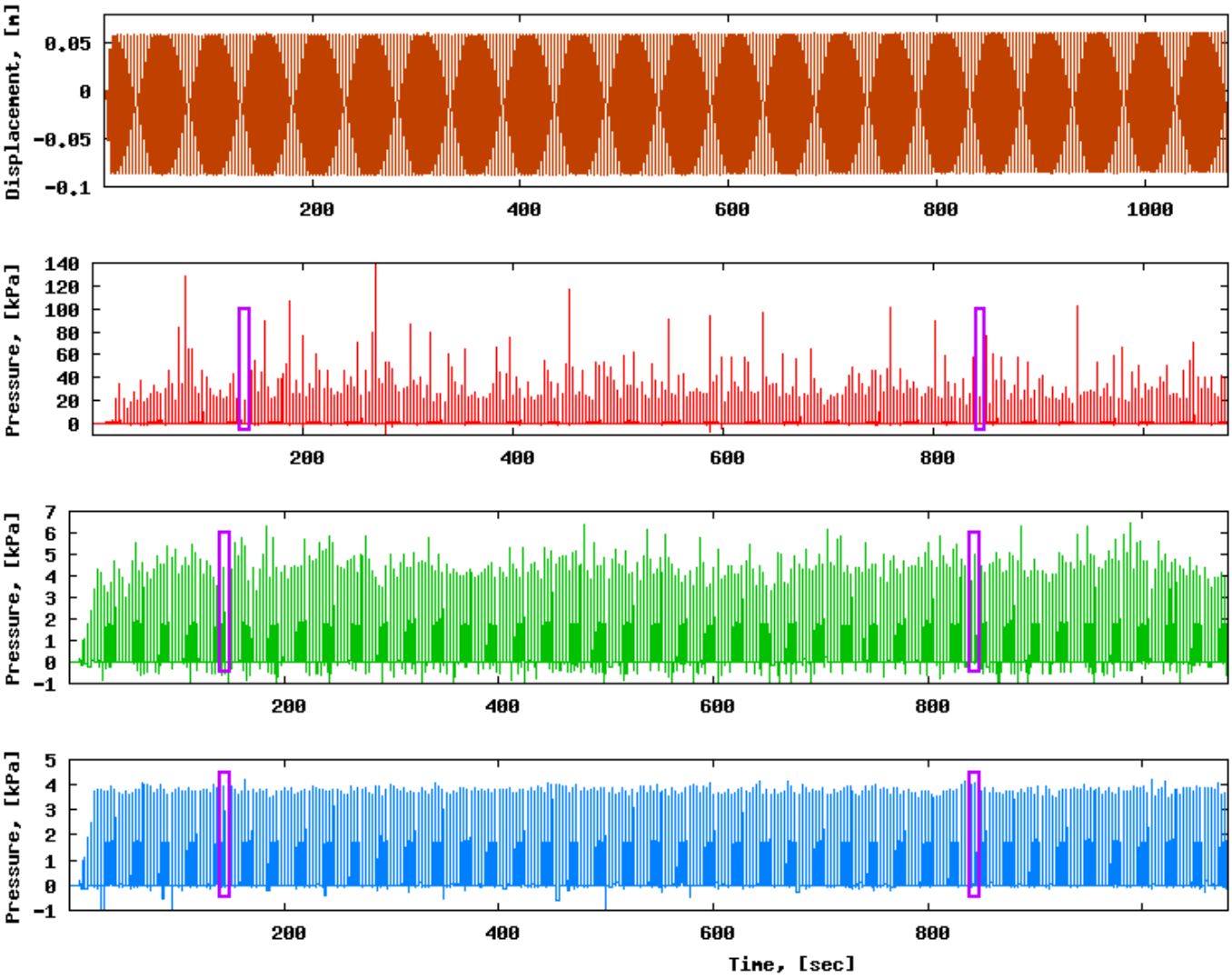

Figure 6. Complete experimental and computational records

FLUID PRESSURES AT P08

The experimental data record for the investigated case has length of just below 19 minutes. The computational runs of 18 min (1080 sec) were performed and complete experimental and computational records for t=0-1080 [sec] are displayed in Fig. 6. Main purpose of this picture is to display a "skyline" of the records, for a visual estimation whether there exists a significant scatter of the extreme values.

The top graph (in brown color) shows experimentally recorded horizontal displacement of the tank and it can be seen that the tank's motion is very stable (and features a stable, graphically induced beat pattern). However, the tank's motion was not ideally sinusoidal due to mechanical imperfections and inertia effects of the laboratory oscillator [4, 15]. The following graph (red color) is the experimental record of fluid pressures at **P08**, while the green and blue graphs show computed pressures from 2D and 3D calculations, respectively. Hereafter, the red, green and blue colors are used consistently in all graphs unless stated otherwise. It is observed that:

- fluid flow excitation (motion of the tank) is stable,
- large scatter of the experimental pressure peak values can be observed,
- there is less scatter in the computational results,
- 3D computational solution is more stable than the 2D one.

Numbers on the vertical pressure axis should not be overlooked; the pressure peaks recorded during the experiment are in much different range of values.

The magenta-colored rectangles in Fig. 6 are exemplary time windows, t=140-149 [sec] and t=840-849 [sec], respectively, and

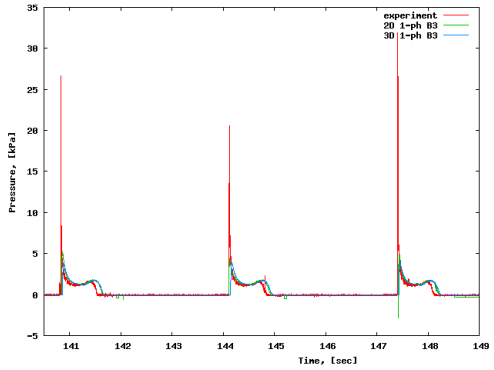

Figure 7. Experimental and computational records, t=140-149 [sec]

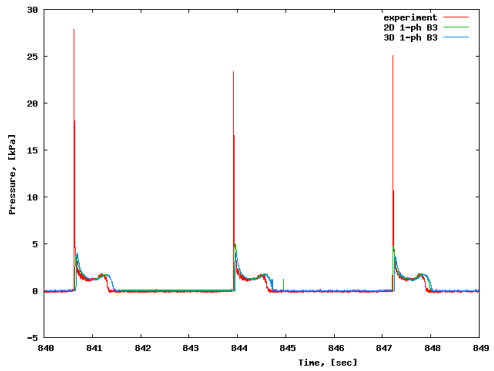

Figure 8. Experimental and computational records, t=840-849 [sec]

each window encloses three pressure peaks. Time traces from these windows are shown in Fig. 7 and Fig. 8, where the experimental and computational graphs have been overlaid. It can be seen that, except for the peak values, there is quite good agreement between laboratory and computer generated data. The computational pressure pulses are close to the experimental ones with regard to time of peak occurence, pulse shape and pulse duration. It is also noted that the ComFLOW simulation is stable even for very long runs; quality of the numerical solution does not deteriorate at all.

Pressure pulses from the entire time records have been collected, synchronised in time to the pressure peak occurence and plotted in the same graph. The experimental data is shown in Fig. 9 and Fig. 10, where in the latter graph a value cut-off has been applied in order to improve legibility of the pressure pulse shape. The thick yellow line on top of the many component curves is the average pressure pulse. Similarly, the component and average pressure pulses obtained from 2D and 3D calculations are displayed in Fig. 11 and Fig. 12, respectively. Again, it can be seen that there is more consistency in 3D computational results.

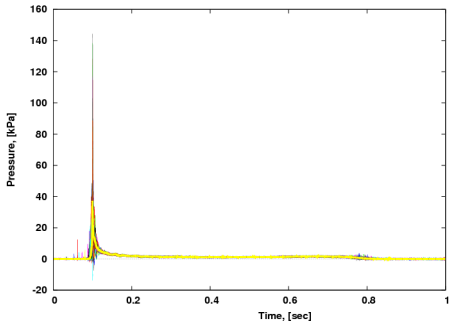

Figure 9. Experimental pressure pulses

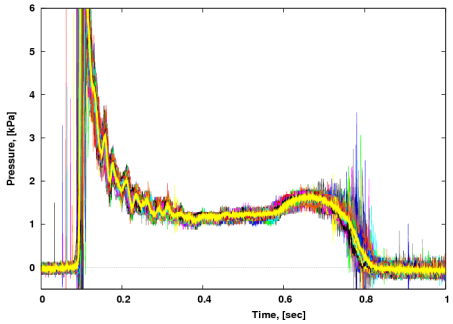

Figure 10. Experimental pressure pulses with 6 [kPa] cut-off

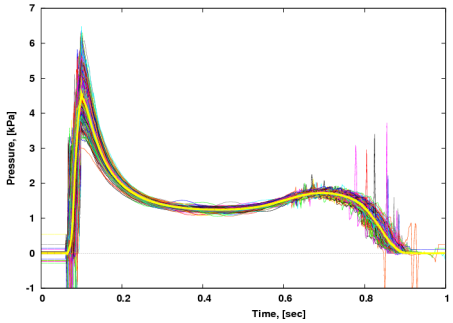

Figure 11. Computational pressure pulses, 2D solution

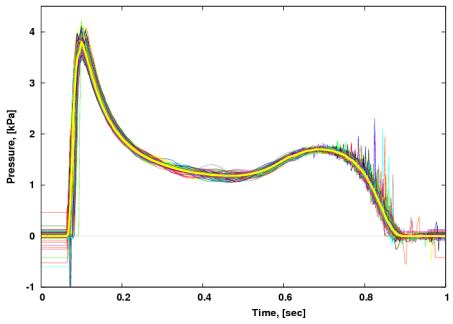

Figure 12. Computational pressure pulses, 3D solution

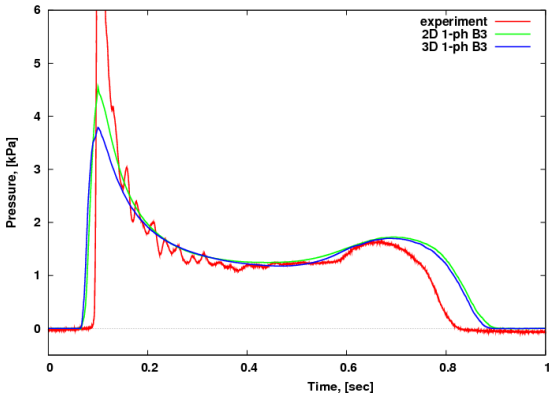

Figure 13. Average pressure pulses with 6 [kPa] cut-off

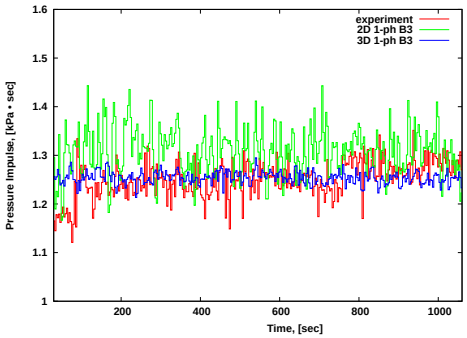

Figure 15. Pressure impulses

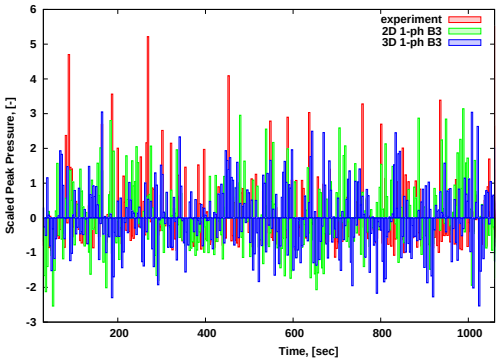

Figure 14. Relative scatter of pressure peaks

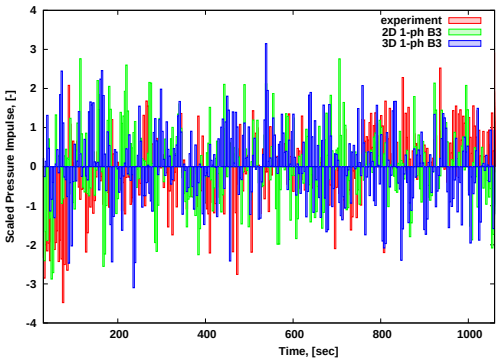

Figure 16. Relative scatter of pressure impulses

PEAK PRESSURE VALUES

It can be concluded from Figs. 9-12 that the pressure pulse shape is rather stable. The average pressure pulses, synchronised in time at the peak's instant occurrence, are shown in Fig. 13 and it appears that the 2D/3D computational pulses are of about the same length, but somewhat longer than the experimental one.

Scatter of the pressure peak values is further presented in Fig. 14 in a more objective form. From the peak values a respective mean peak value was subtracted and the result was scaled by a respective standard deviation value (see Table 1). It can be noticed that, except for several large experimental (relative) peaks, the relative scatter is about the same for the experiments and calculations, at least visually.

PRESSURE IMPULSE VALUES

The pressure signal can be integrated in time over duration of one pulse to produce a single number, hereafter denoted as *pressure impulse*. The pressure impulse is one of relevant parameters for dynamical structural response estimation.

Values of the pressure impulses are shown in Fig. 15, while their relative scatter, obtained in a similar way as the relative scatter of pressure peaks, is presented in Fig. 16. Table 2 can be consulted for values of means and standard deviations. It is observed that:

- the pressure impulse values are in the same range for experiment and calculations (recall that values of experimental and computational pressure peaks differed significantly). This indicates that although the experimental peaks reach high values, their duration is very short and the peaks contribute little to the impulse value. It is also noted that the 2D calculations produce the largest pressure impulses,
- relative scatter of the pressure impulses is again about the same for the experiments and calculations, this observation is found by a visual inspection of Fig. 16.

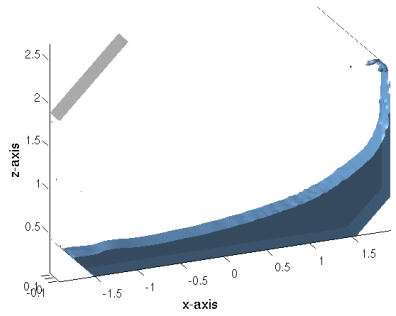

Figure 17. Frame from the 3D simulation at t=144.6 [sec]

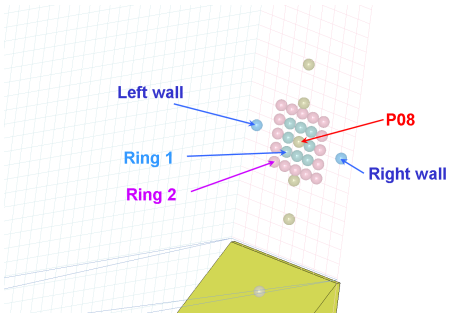

Figure 18. Panel of computational sensors for 3D calculations

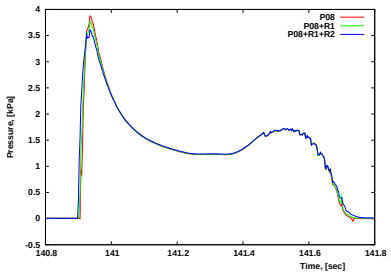

Figure 19. 3D effects: ring-averaged pressures

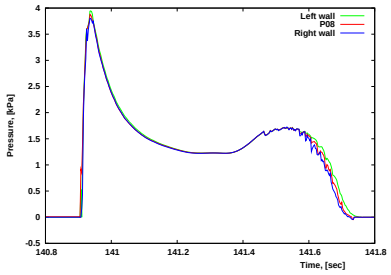

Figure 20. 3D effects: pressures at wall points

MORE ABOUT 3D EFFECTS

The pre-assumption of flow two-dimensionality for the considered geometry is inspected further. An example of the computed 3D fluid configuration is displayed in Fig. 17 and there are no clearly visible deviations from the two-dimensionality, perhaps except at the up-wall jet.

Fig. 18 shows a close-up of the sub-panel of computational pressure sensors placed near the **P08** point. There are two surrounding layers of control points forming *rings* and two more control points close to the walls.

Pressure pulses were averaged over either 9 control points (**P08**, Ring 1), or over 25 points (**P08**, Ring 1, Ring 2). The results are shown in Fig. 19 and it is observed that such derived curves nearly overlap. The peak value decreases slightly and the pressure pulse widens a bit, as expected (both effects due to small differences in arrival time at the sub-panel control points).

Another approach is presented in Fig. 20, where the time-pressure functions at **P08** and near-wall points are shown. Again, the curves nearly overlap.

STATISTICAL DESCRIPTION

The considered time-pressure series contain approximately $N \approx 330$ pressure pulses and it is justified to employ some statistical tools. Basic statistical parameters of the considered data sets are listed in Tables 1 and 2, where excess kurtosis value is given. Several observations are offered:

- the characteristic pressure peak values: maximum, mean and median are much higher for experimental data than for the calculations,
- respective mean and median values are very similar for both peaks and impulses, which suggests that number of "outlier" data points is limited. An exception is the experimental peak pressure data set, where there is a $\sim 20\%$ mean vs. median difference, indicating presence of the "outlier" points,
- skewness value for the experimental peak pressure data set is large, > 2. This suggests asymmetry of the probability distribution function (PDF); the positive value indicates a tail extending towards positive values. These observations are confirmed by the binned data graph, Fig. 21, where a rather long tail in high value range can be seen,
- the experimental peak pressure data record features large kurtosis. The kurtosis value is a measure of the *peakedness* of the PDF. This fact has already been noticed, and again is confirmed in Fig. 21,
- computational pressure peaks have much smaller skewness and kurtosis. Their probability distribution functions do not

feature significant asymmetry and long tails, see Figs. 22 and 23. Numbers along the horizontal axes of these graphs indicate that 3D calculations produce less scatter of the pressure peaks than 2D calculations (but note that now the scatter values are absolute - in [kPa], not scaled),

- pressure impulse data sets from the experiments and 2D/3D calculations are much more consistent between themselves. Maximum, mean and median values are all in the same range. In particular, the respective mean and median values are almost exactly the same,
- the experimental pressure impulses feature the largest skewness and kurtosis, but the values are much smaller than for the experimental pressure peaks.

Table 1. Statistical parameters of pressure peaks

Parameter	Unit	Experiment	Comp-2D	Comp-3D
Max. value	kPa	144.31	6.488	4.204
Mean	kPa	37.24	4.564	3.794
Median	kPa	30.79	4.471	3.790
Std. dev.	kPa	19.37	0.612	0.135
Skewness	-	2.33	0.579	0.233
Kurtosis	-	7.03	0.439	-0.00322

Table 2. Statistical parameters of pressure impulses

Parameter	Unit	Experiment	Comp-2D	Comp-3D
Max. value	kPa·sec	1.367	1.443	1.295
Mean	kPa·sec	1.254	1.308	1.254
Median	kPa·sec	1.256	1.308	1.254
Std. dev.	kPa·sec	0.0384	0.0491	0.0131
Skewness	-	-0.426	0.0285	-0.0591
Kurtosis	-	0.454	0.191	0.0709

Binning of Data and PDF Histograms

A set of six histograms is presented, Figs. 21-26. The probability distribution functions (PDF) have been created by data binning, which is a basic technique used to reduce effects of minor statistical defects in processed data sets. It is known that different bin sizes can reveal different features of the considered data and a truly objective width of bins can be difficult to find.

In this paper, bin sizes used to create the presented PDFs were established from Freedman & Diaconis rule [16]:

$$\textbf{Bin size} \;=\; 2 \cdot \textbf{IQR}(x) \cdot N^{-1/3} \qquad (3)$$

where x is a vector of data values, $\textbf{IQR}(x)$ is the interquartile range of the data vector, and N is the number of observations. The interquartile range **IQR** is a measure of statistical dispersion and is the difference between the third and first quartiles (median values in data sub-sets). The interquartile range is considered a robust statistic [16].

A consistently established number of the necessary bins can be itself an estimator of the data spread. Table 3 shows that the experimental peaks' data set is the outstanding one:

Table 3. Number of necessary bins, Freedman & Diaconis rule

	Experiment	Comp-2D	Comp-3D
Pressure peaks	27	17	15
Pressure impulses	19	17	17

CONCLUSIONS

A statistically-oriented analysis of long CFD computational runs simulating sloshing in a tank was presented and results were compared with the available experimental data. One exemplary experimental data set, of regular excitation sloshing with 10 % tank fill ratio, was investigated.

The authors are aware that all stated observations are of limited generality, but the research is considered as a preliminary one and will be continued in future. It is concluded that:

1. Both 2D and 3D computations seem to be able to reproduce the experimental pressure pulse shape, but are *not* capable of reproducing high values of the experimental pressure peaks.
2. The 2D/3D calculations were performed with a uniform grid of size around δ=0.03 [m], or $\sim$1/130 of the tank length. There exists an evidence that 2D calculations with 3$\times$ higher grid resolution (δ=0.01 [m], or $\sim$1/400 of the tank length) can produce higher pressure peaks, while the pressure pulse shape remains unchanged [4, 11]. However, the performed computational runs with δ=0.03 [m], reported in this article, took days to complete and estimations are that solution with a denser grid is currently un-obtainable computationally to the authors, especially in 3D. This path of inquiry will be pursued in future.
3. The related problem could be the computational time step and perhaps missed pressure peak instants. Experimental pressures were recorded at a constant sampling rate of 10 kHz or with Δt=10^{-4} [sec], while the ComFLOW computational time step varies, since it is continuously adjusted as the simulation proceeds (due to time integration scheme stabilitity constraints). For results reported in this paper, the average ComFLOW time steps were several times larger than the experimental sampling rate, $\Delta t^{(2D)}$=5.69·10^{-4} [sec] and $\Delta t^{(3D)}$=3.85·10^{-4} [sec], respectively.
4. An additional inspection of the simulated 3D flow results revealed that fluid behaves essentially in a 2D manner. The

undertaken pre-assumption of the flow two-dimensionality seems to hold, at least for the considered geometry and tank fill rate.

5. An interesting result from the 3D simulation (of the essentially 2D flow) is that 3D peak pressures are clearly smaller than in the corresponding 2D simulation test (on average, by $\sim$20%).
6. The experimentally obtained pressure impulse values are much better predicted by the computational means, in particular by the 3D simulation. The 2D calculations slightly over-predict.
7. It is possible to fit some popular theoretical probability distribution functions to the presented binned PDFs, both experimental and computational. Good candidates seem to be Weibull distribution with respect to Fig. 21, and normal distribution with respect to Figs. 22-26.
8. Some random scatter of experimental results is typically expected, and this would be the case especially for the problem at hand (hydrodynamic impact measurements). However, it looks like the 2D/3D sloshing calculations are *not* entirely deterministic. Sensitivity studies with respect to small changes in exctitation can cast some light on the problem. Yet, the authors have already performed a similar calculation with a purely sinusoidal excitation, and scattered peak pressure values were predicted [5].

The authors believe that the presented study can be of value for the sloshing problem researchers' community. Due to space limitations, it was not possible to include all material available at the time of writing. More results, including repeated runs to stabilize the statistical parameters, and with higher tank filling rates will be published in future.

ACKNOWLEDGMENT

Authors would like to thank participants of the ComFLOW-2 Joint Industry Project for permission to publish the experimental results.

REFERENCES

[1] Yu, K., Chen, H-C., Kim, J.W., and Lee, Y-B., 2007. "Numerical Simulation of Two-Phase Sloshing Flow in LNG Tank Using Finite-Analytic Level-Set Method". In Proceedings, 26-th International OMAE Conference, San Diego, CA. Paper OMAE2007-29745.

[2] Peric, M., Zorn, T., El Moctar, O., Schellin, T.E, and Kim, Y-S., 2007. "Simulation of Sloshing in LNG-Tanks". In Proceedings, 26-th International OMAE Conference, San Diego, CA. Paper OMAE2007-29555.

[3] Wemmenhove, R., Luppes, R., Veldman, A.E.P., and Bunnik, T., 2008. "Application of a VOF Method to Model Compressible Two-Phase Flow in Sloshing Tanks". In Proceedings, 27-th International OMAE Conference, Estoril, Portugal. Paper OMAE2008-57254.

[4] Iwanowski, B., Lefranc, M., and Wemmenhove, R., 2009. "Numerical Simulation of Sloshing in a Tank, CFD Calculations Against Model Tests". In Proceedings, 28-th International OMAE Conference, Honolulu, Hawaii, USA. Paper OMAE2009-79051.

[5] Wemmenhove, R., Iwanowski, B., Lefranc, M., Veldman, A.E.P., Luppes, R., and Bunnik, T., 2009. "Simulation of Sloshing Dynamics in a Tank by an Improved Volume-of-Fluid Method". In Proceedings, 19-th International ISOPE Conference, Osaka, Japan. Paper YHK-05.

[6] Schreier, S., Godderidge, B., Paschen, M., Turnock, S., Tan, M., and Cowlan, N., 2009. "Assessment of Transient Sloshing Due to Encounter of an LNG Carrier With a Steep Wave". In Proceedings, 28-th International OMAE Conference, Honolulu, Hawaii, USA. Paper OMAE2009-79080.

[7] ISOPE SDD, 2009. "First ISOPE Sloshing Dynamics and Design Symposium". In Proceedings, 19-th International ISOPE Conference, Osaka, Japan.

[8] Hirt, C.W., and Nichols, B.D., 1981. "Volume Of Fluid (VOF) Method for the Dynamics of Free Boundaries". *Journal of Computational Physics,* **39**, pp. 201–225.

[9] Maritime Research Institute Netherlands (MARIN). Joint Industry Projects Web Page, `www.marin.nl/web/JIPs-Networks.htm`.

[10] Wemmenhove, R., 2008. "Numerical Simulation of Two-Phase Flow in Offshore Environments". PhD Thesis, University of Groningen, The Netherlands, May.

[11] Iwanowski, B., 2008. ComFLOW-2 JIP: Benchmarks of the ComFLOW Program. Technical Report TR-2008-0049, FORCE Technology Norway AS, Sandvika, Norway, October.

[12] Bunnik, T.H.J., 2007. Large Scale Sloshing Model Tests. Technical Report 18378-1-PO, Maritime Research Institute Netherlands (MARIN), Wageningen, The Netherlands, August.

[13] Kleefsman, K.M.T., 2005. "Water Impact Loading on Offshore Structures - A Numerical Study". PhD Thesis, University of Groningen, The Netherlands, November.

[14] Kleefsman, K.M.T., Fekken, G., Veldman, A.E.P., Buchner, B., and Iwanowski, B., 2005. "A Volume-Of-Fluid Based Simulation Method for Wave Impact Problems". *Journal of Computational Physics,* **206**, pp. 363–393.

[15] Bunnik, T., and Huijsmans, R., 2007. "Large Scale LNG Sloshing Model Tests". In Proceedings, 17-th International ISOPE Conference, Lisbon, Portugal.

[16] Freedman, D., and Diaconis, P., 1981. "On the Histogram as a Density Estimator: L2 Theory". *Probability Theory and Related Fields,* **57**(4), pp. 453–476.

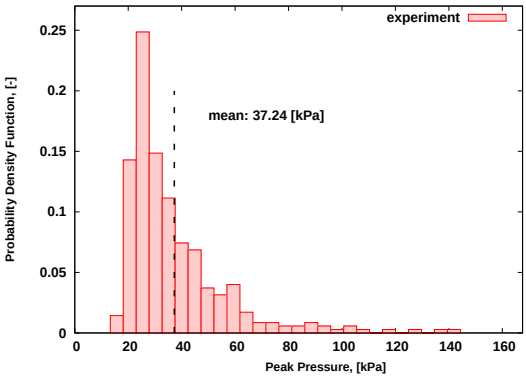

Figure 21. Binned pressure peaks, experiment

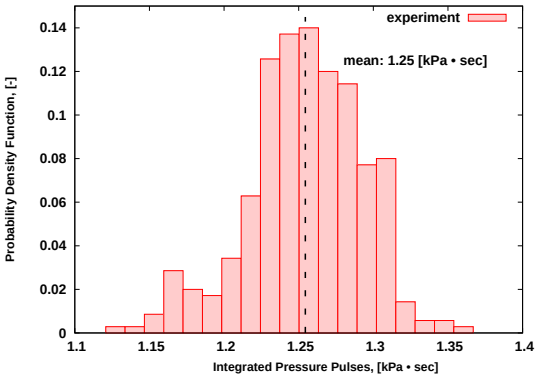

Figure 24. Binned pressure impulses, experiment

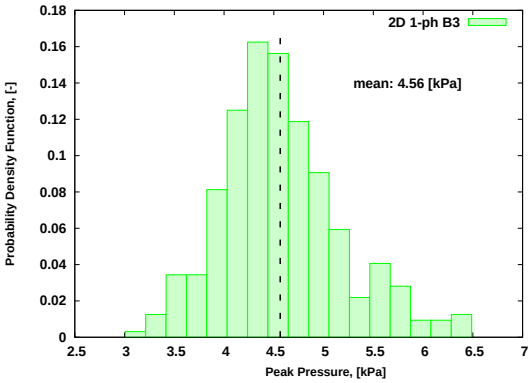

Figure 22. Binned pressure peaks, 2D calculation

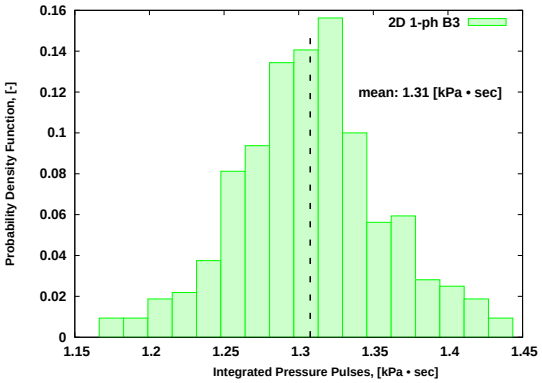

Figure 25. Binned pressure impulses, 2D calculation

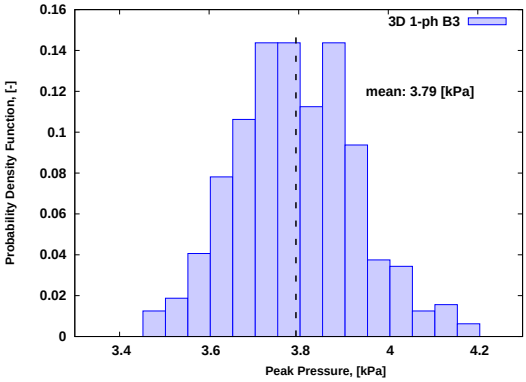

Figure 23. Binned pressure peaks, 3D calculation

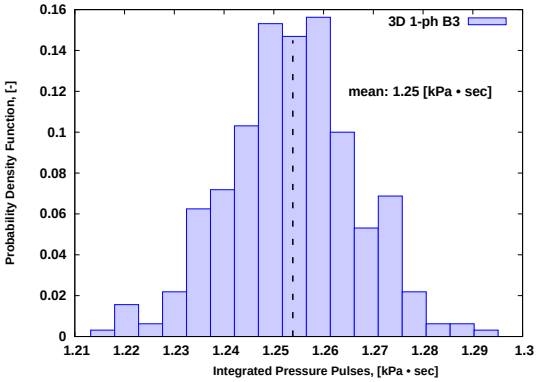

Figure 26. Binned pressure impulses, 3D calculation